

Evidence of bar–driven secular evolution in the gamma–ray narrow–line Seyfert 1 galaxy FBQS J164442.5+261913

A. Olguín–Iglesias,^{1,2*} J. K. Kotilainen,² J. León Tavares,³ V. Chavushyan¹ C. Añorve⁴

¹*Instituto Nacional de Astrofísica Óptica y Electrónica (INAOE), Apartado Postal 51 y 216, 72000 Puebla, México;*

²*Finnish Centre for Astronomy with ESO (FINCA), University of Turku, Väisäläntie 20, FI-21500 Piikkiö, Finland*

³*Sterrenkundig Observatorium, Universiteit Gent, Krijgslaan 281-S9, B-9000 Gent, Belgium*

⁴*Facultad de Ciencias de la Tierra y del Espacio de la Universidad Autónoma de Sinaloa, Blvd. de las Américas y Av. Universitarios S/N, Ciudad Universitaria, C.P. 80010, Culiacán Sinaloa, México*

Accepted XXX. Received YYY; in original form ZZZ

ABSTRACT

We present near–infrared (NIR) imaging of FBQS J164442.5+261913, one of the few γ –ray emitting Narrow Line Seyfert 1 (NLSy1) galaxies detected at high significance level by *Fermi*–LAT. This study is the first morphological analysis performed of this source and the third performed of this class of objects. Conducting a detailed two–dimensional modeling of its surface brightness distribution and analysing its $J - K_s$ colour gradients, we find that FBQS J164442.5+261913 is statistically most likely hosted by a barred lenticular galaxy (SB0). We find evidence that the bulge in the host galaxy of FBQS J164442.5+261913 is not classical but pseudo, against the paradigm of powerful relativistic jets exclusively launched by giant ellipticals. Our analysis, also reveal the presence of a ring with diameter equalling the bar length ($r_{bar} = 8.13 \text{ kpc} \pm 0.25$), whose origin might be a combination of bar–driven gas rearrangement and minor mergers, as revealed by the apparent merger remnant in the J –band image. In general, our results suggest that the prominent bar in the host galaxy of FBQS J164442.5+261913 has mostly contributed to its overall morphology driving a strong secular evolution, which plays a crucial role in the onset of the nuclear activity and the growth of the massive bulge. Minor mergers, in conjunction, are likely to provide the necessary fresh supply of gas to the central regions of the host galaxy.

1 INTRODUCTION

Narrow line Seyfert 1 (NLSy1) galaxies are type 1 active galactic nuclei (AGN) characterized by narrower Balmer lines ($FWHM(H\beta) < 2000 \text{ km s}^{-1}$) than in normal Seyferts, flux ratios $[OIII]/H\beta < 3$, strong optical FeII lines (FeII bump) and a soft X-ray excess (Osterbrock & Pogge 1985; Pogge 2000). Based on the full width at half maximum (FWHM) of their Broad Line Region (BLR) lines and the continuum luminosity (Kaspi et al. 2000), their central black holes masses (M_{BH}) are estimated to range from $\sim 10^6 M_\odot$ to $\sim 10^7 M_\odot$ (Mathur et al. 2012a, although Baldi et al. 2016 show that these low M_{BH} estimates might be seriously affected by the orientation of the BLR). Their low–mass black holes suggest that their accretion rates are close to the Eddington limit and their host galaxies are in an early phase of galaxy evolution (Ohta et al. 2007). Unfortunately, relatively little is known about their host galaxies.

Some studies find that their morphologies resemble those of inactive spirals with a regular presence of stellar bars (Crenshaw et al. 2003a), and pseudobulges (Orban de Xivry et al. 2011; Mathur et al. 2012b). However, γ –ray emission have been detected in seven radio–loud NLSy1

(RL–NLSy1) by the Large Area Telescope (LAT) on board the *Fermi* satellite, suggesting that highly beamed and strongly collimated relativistic jets can be launched by RL–NLSy1 AGN. The latter, challenge the paradigm that such jets are launched exclusively by blazars hosted by giant elliptical galaxies (Laor 2000; Marscher 2009) with black holes with masses $M_{BH} \gtrsim 10^8 M_\odot$ accreting at low rates (McLure et al. 2004; Sikora et al. 2007). Therefore, a thorough analysis of the host galaxies of this new class of AGN (hereafter γ –NLSy1, Abdo et al. 2009), becomes a priority.

So far, only two γ –NLSy1 host galaxies have been characterized, 1H 0323+342 (Antón et al. 2008; León Tavares et al. 2014) and PKS 2004–447 (Kotilainen et al. 2016). These studies reveal characteristics such as the presence of disks, rings, bars and pseudobulges, which are expected in normal NLSy1s, however, do not fit with the common belief that powerful relativistic jets are launched exclusively by giant ellipticals.

As part of our ongoing imaging survey of the complete sample of γ –NLSy1 galaxies detected so far, we conducted NIR (J and K_s –bands) observations to the γ –NLSy1 FBQS J164442.5+261913. This is one of the sources detected

by *Fermi*-LAT with high significance, having test statistic $TS > 25$ ($\sim 5\sigma$, [Matttox et al. 1996](#)) and given its redshift ($z = 0.145$, [Bade et al. 1995](#)), it is the second closest after 1H 0323+342 ($z = 0.061$), making it an excellent candidate for accurate morphological studies to its host galaxy. With the aim of achieving a better understanding of the mechanisms needed to form and develop highly collimated relativistic jets, in this paper we present the results from our thorough analysis to FBQS J164442.5+261913.

This paper is structured as follows: Observations and data reduction are presented in Section 2; the methods we adopt to analyse the data are explained in Section 3. Our results and discussion are presented in Section 4 and 5. In Section 6 we summarize our findings. Throughout the manuscript we adopt a concordance cosmology with $\Omega_m = 0.3$, $\Omega_\Lambda = 0.7$ and a Hubble constant of $H_0 = 70 \text{ Mpc}^{-1} \text{ km s}^{-1}$.

2 OBSERVATIONS AND DATA REDUCTION

The *J*- and *K*-band observations of FBQS J164442.5+261913 were conducted at the 2.5 m Nordic Optical Telescope (NOT) during the night of May 1, 2015 using the Wide-Field near-infrared camera NOTcam with CCD dimensions of $1024 \text{ pix} \times 1024 \text{ pix}$ and a pixel scale of $0.234''/\text{pix}$, giving a field of view of $\sim 4 \times 4 \text{ arcmin}^2$. During the night, the seeing was very good, with an average FWHM of $\sim 0.75''$ and $\sim 0.63''$ for *J*- and *K_s*-bands, respectively. The target was imaged using the NOTcam standard *J* ($\lambda_{\text{central}} = 1.246 \mu\text{m}$) and *K_s* ($\lambda_{\text{central}} = 2.140 \mu\text{m}$) filters with a dithering technique with individual exposures of 30 seconds and a typical offset of $\sim 10''$. A total of 85 individual exposures for *J*-band and 72 for *K_s*-band were obtained, giving a total exposure time of 2550 seconds and 2160 seconds, respectively.

The data reduction was performed using the NOTcam reduction package¹ for IRAF². First we corrected for the optical distortion of the Wide-Field camera using distortion models based on high quality data of a stellar-rich field. Then, bad pixels were masked out using a file available in the NOTCam bad pixel mask archive. A normalized flat field was created from evening and morning sky frames to account for the thermal contribution. Using field stars as reference points, the dithered images were aligned and co-added to obtain the final reduced image used in our analysis. In order to perform photometric calibration to the images, we retrieved *J*- and *K_s*- band magnitudes from 2MASS ([Skrutskie et al. 2006](#)) resulting in an accuracy of $\sim 0.10 \text{ mag}$. The derived integrated magnitudes in circular apertures are $m_J = 15.35 \pm 0.10$ ($M_J = -23.84 \pm 0.10$) and $m_{K_s} = 13.44 \pm 0.10$ ($M_{K_s} = -25.86 \pm 0.10$). Galactic extinction for *J* and *K_s* bands are negligible ($A_\lambda[J] = 0.058$ and $A_\lambda[K_s] = 0.025$).

¹ www.not.iac.es/instruments/notcam/

² IRAF is distributed by the National Optical Astronomy Observatories, which are operated by the Association of Universities for Research in Astronomy, Inc., under cooperative agreement with the National Science Foundation

3 IMAGE ANALYSIS

3.1 Photometric decomposition

We perform a 2D modeling of the galaxy using the image decomposition code GALFIT ([Peng et al. 2011](#)). We follow the procedure described in our previous studies of AGN host galaxies ([León Tavares et al. 2014](#); [Olguín-Iglesias et al. 2016](#)), which is described below.

The first, and most important part of the analysis is the modeling of the point spread function (PSF) by fitting selected stars of the field of view (FOV, Fig. 1). These stars are non-saturated, with no sources within $\sim 7''$ radius, more than $\sim 10''$ away from the border of the FOV and with a range of magnitudes that allow us a proper characterization of core and wings. Stars 2, 5, 6, 8 and 9 fulfil these criteria (see Figure 1) and thus are used to derive our PSF model. On the other hand, star 1 is saturated, stars 3 and 10 are very close to the border of the FOV and stars 4 and 7 have close companions.

Each selected star is centered in a $50'' \times 50''$ box, where all extra sources are masked out by implementing the segmentation image process of SExtractor ([Bertin & Arnouts 1996](#)). The stars are simultaneously modeled, using one Gaussian function (intended to fit the core of the stars) then, the resulting model is added with an exponential function (intended to fit the wings of the stars). Similarly, depending on the residuals, we add extra Gaussians and exponential functions until the core and wings are satisfactorily fitted. For our imagery, six Gaussians and six exponentials (and a flat plane, that fits the sky background) were enough. The result is considered as a suitable PSF model for our analysis once it successfully fits all the stars individually (Figure 2).

Next, we fit FBQS J164442.5+261913 with the scaled version of our derived PSF as the only component, to constrain the unresolved AGN contribution at the centre of the galaxy. Since the residuals of the single PSF model (hereafter model 1) are considerable ($\chi_{\text{model1}}^2 = 4.148 \pm 0.01$ for *J*-band and $\chi_{\text{model1}}^2 = 3.171 \pm 0.02$ for *K_s*-band), we continue our analysis by adding extra functions to the model. We use the Sérsic profile, expressed such that

$$I(R) = I_e \exp \left[-\kappa_n \left(\left(\frac{R}{R_e} \right)^{1/n} - 1 \right) \right] \quad (1)$$

where $I(R)$ is the surface brightness at the radius R , and κ_n is a parameter coupled to the Sérsic index n in such a way that I_e is the surface brightness at the effective radius R_e , where the galaxy contains half of the light ([Graham & Driver 2005](#)). The Sérsic profile has the ability to represent different stellar distributions such as elliptical galaxies, classical- and pseudo-bulges and bars, just by varying its Sérsic index n . Hence, when $n = 4$, the Sérsic function is known as the de Vaucouleurs profile (widely used to fit elliptical galaxies and classical bulges); when $n = 1$, it is an exponential function, and when $n = 0.5$, it is a Gaussian.

Given that NLSy1s are known to be typically hosted in disc galaxies ([Crenshaw et al. 2003b](#)), we also explore models that include the exponential function, expressed as:

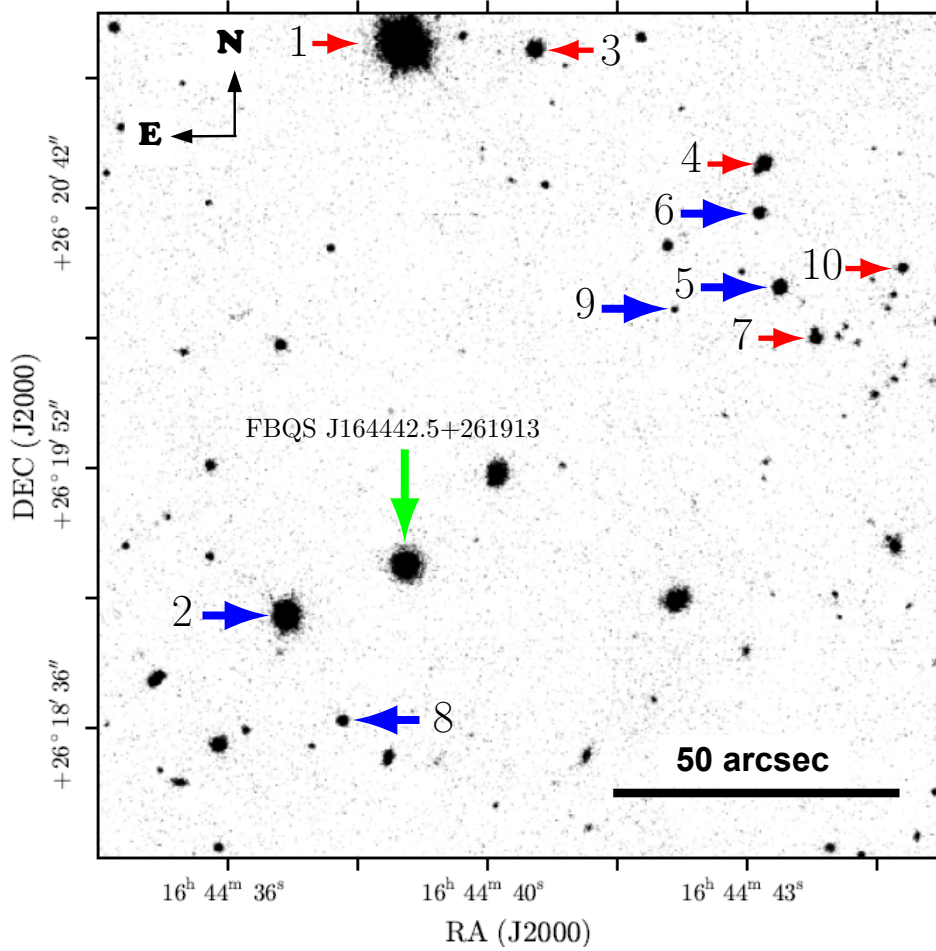


Figure 1. J -band NOTcam image of FBQS J164442.5+261913. The large green vertical arrow indicates the location of the target. Horizontal arrows show the suitable (blue thick arrows) and unsuitable (red thin arrows) stars for the PSF construction.

$$I(R) = I_0 \exp\left(-\frac{R}{h_r}\right) \quad (2)$$

where $I(R)$ is the surface brightness at the radius R , I_0 is the central surface brightness and h_r is the disc scale length.

3.1.1 Uncertainties

Since the error bars produced by GALFIT are purely statistical and thus, unrealistically small (Häussler et al. 2007; Bruce et al. 2012), we follow Kotilainen et al. (2011) and León Tavares et al. (2014) to derive the uncertainties of our fittings. We identify model parameters that could contribute most significantly to errors. Regarding the PSF, spatial variations might affect the structural parameters of the galaxy model and, to a lesser extent, its magnitudes. To account for this, we compare the brightness distribution of our PSF model with the brightness distribution of each star in the field, whose only difference is assumed to lie in their positions.

On the other hand, sky background can affect magnitudes in a larger extent (when compared to the PSF) and to

a lesser extent (yet significantly), the structural parameters of the galaxy model. Even though, our imagery is in NIR bands and thus the sky counts are SKYCOUNTS ≈ 0 , they may show large variations. To account for this, we run several sky fits in separated regions of 300 pixels \times 300 pixels (70" \times 70") and use the mean and $\pm 1\sigma$ of the resultant values to fit the galaxy. The outcomes are models with slightly different magnitudes which are assumed to be the errors due to the sky background.

Model magnitudes are also affected by uncertainties in the zero-point, estimated from magnitudes retrieved from 2MASS. Thus, zero-point magnitude variations (± 0.1 mag) are also added as errors in the magnitudes of our final models.

3.2 Fit of the isophotes

Additionally to the morphological decomposition, we perform an analysis based on the ellipse fit to the galaxy isophotes (Wozniak et al. 1995; Knapen et al. 2000; Laine et al. 2002; Sheth et al. 2003; Elmegreen et al. 2004; Marinova & Jogee 2007; Barazza et al. 2008). We perform this analysis using the *ELLIPSE* task in IRAF. This procedure

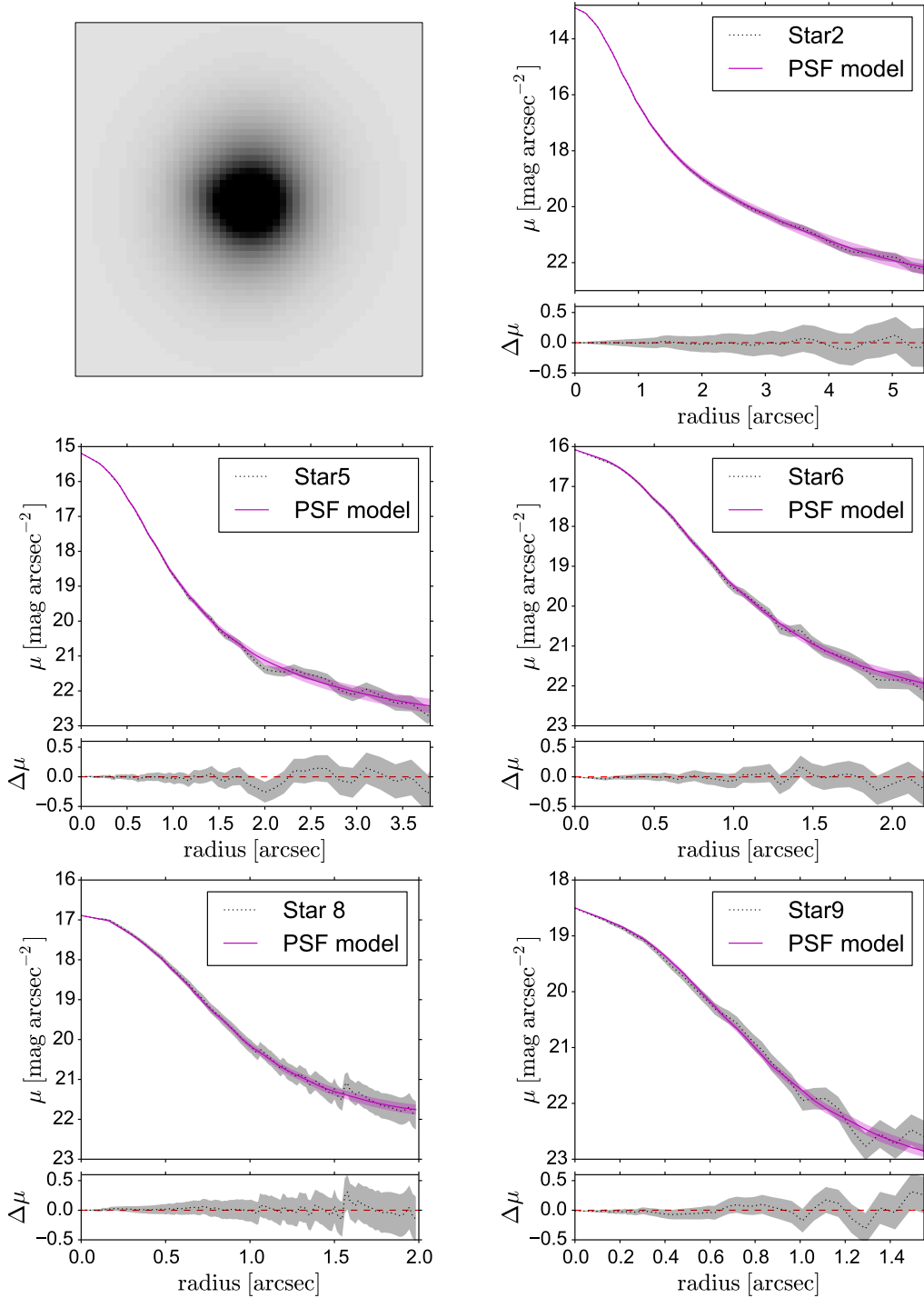


Figure 2. Test of the PSF model (top left image). Each star is fitted with our final PSF model in order to ensure its reliability. The top subpanel of each plot shows the azimuthally averaged surface brightness profiles of the PSF model (magenta line) and the fitted star (black data points). The lower subpanel shows the residuals of the fit.

reads a 2-dimensional image to fit isophotes to its light distribution. The fits start from an initial guess of x and y center, ellipticity (ϵ) and position angle (PA). Each extracted isophote is represented by its surface brightness (μ), semi-major axis length (R), PA and ϵ .

The fitted isophotes are used to represent and analyse the azimuthally averaged surface brightness profiles of the

galaxy and the models derived from the photometric decomposition. Furthermore, the sample of isophotes extracted are used to identify changes in PA and ellipticity that could be associated to different structures within the galaxy morphology.

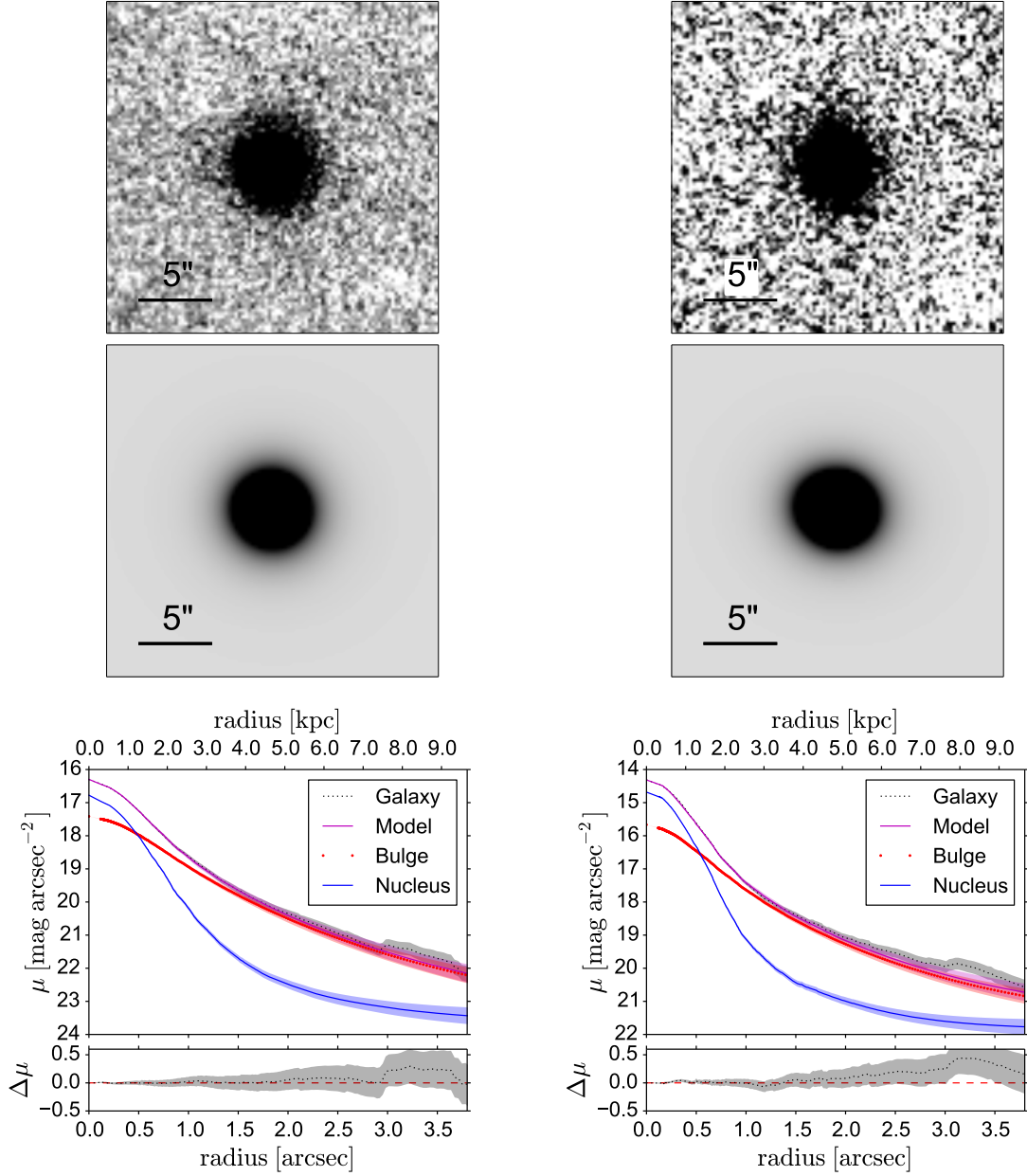


Figure 3. Model 2 (AGN+Bulge). North is up and east is to the left. Left column shows the J -band and right column shows the K_s -band. Top row shows the observed images. Middle row shows the models images. Lower row shows the azimuthally averaged surface brightness profiles of the target, the model and the subcomponents of the model (top panel) and its residuals (bottom panel). Symbols are explained in the plots.

4 STRUCTURE OF FBQS J164442.5+261913

In order to characterize the morphology of FBQS J164442.5+261913, we first assume that it is hosted by an elliptical galaxy, since only these type of galaxies are known to launch powerful relativistic jets able to produce γ -rays (Marscher 2009). Thus, we add a Sérsic profile to the single PSF model that represents the AGN contribution. We constrain the Sérsic index to $n > 2.0$, given the observational evidence that the light profiles of most ellipticals and classical bulges, are better described by a Sérsic function with

$n > 2$, whereas most disk-like bulges have $n < 2$ (Fisher & Drory 2008; Gadotti 2009).

By means of a χ^2 test, we find that the improvement of this model (hereafter model 2) is equal for the J - and the K_s -bands ($\chi^2_{model2}/\chi^2_{model1} = 0.42$ for J -band and $\chi^2_{model2}/\chi^2_{model1} = 0.42$ for K_s band). The images of the galaxy and the models, as well as the azimuthally average surface brightness profiles of the galaxy, the model and the sub-components of the model for each band are shown in Figure 3.

The residual image of the J -band from model 2 (top

Parameter	Model 1		Model 2		Model 3		Model 4 ^a
	<i>J</i>	<i>K_s</i>	<i>J</i>	<i>K_s</i>	<i>J</i>	<i>K_s</i>	<i>K_s</i>
m_{AGN}	15.65 (0.33)	14.28 (0.34)	16.67 (0.38)	14.39 (0.41)	16.67 (0.43)	14.80 (0.38)	14.38 (0.24)
m_{bulge}	-	-	15.70 (0.37)	13.86 (0.39)	17.77 (0.40)	14.55 (0.39)	14.97 (0.32)
m_{disc}	-	-	-	-	16.28 (0.35)	14.33 (0.38)	14.90 (0.25)
m_{bar}	-	-	-	-	-	-	15.32 (0.42)
R_{eff} ["/kpc]	-	-	0.95/2.40 (0.23/0.58)	0.82/2.07 (0.27/0.68)	0.38/0.96 (0.13/0.32)	0.30/0.76 (0.14/0.35)	0.43/1.10 (0.14/0.34)
h_r ["/kpc]	-	-	-	-	2.62/6.65 (0.45/1.14)	3.04/7.68 (0.40/1.01)	3.19/8.10 (0.47/1.20)
n_{bulge}	-	-	2.58 (0.40)	2.71 (0.42)	1.80 (0.31)	1.95 (0.38)	1.90 (0.35)
n_{bar}	-	-	-	-	-	-	1.17 (0.30)
ϵ_{bar}	-	-	-	-	-	-	0.59 (0.06)
χ^2_{ν}	4.250 (0.032)	3.927 (0.033)	1.785 (0.030)	1.645 (0.031)	1.160 (0.027)	1.300 (0.029)	1.181 (0.022)

Table 1. Best-fit parameters for model 1 (PSF only), model 2 (PSF+bulge), model 3 (PSF+bulge+disk) and model 4 (PSF+bulge+disk+bar). Parameter errors appear in parentheses^b.

^a Model 4 is only shown for *K_s*-band, since no stellar bar is detected in *J*-band.

^b Parameter errors are estimated following procedure from section 3.1.1.

panel of Figure 4), shows a ring like feature interrupted in the eastern part. Neither the residuals nor the surface brightness profiles of the stars fitted with our PSF model show similar features. Moreover, its radius ($\sim 3.5''$) exceeds by far the FWHM of our PSF ($\sim 0.75''$). Hence, we consider the ring as a real component of the host galaxy.

The *K_s*-band residual (top panel of Figure 5) shows an elongated and roughly symmetric structure with a length similar to the diameter of the ringed feature ($\sim 3.2''/\sim 8.1$ kpc). In both bands a not-fitted bump in the light distribution of the galaxy is observed (from $\sim 2.8''$ to $\sim 3.7''$), which is consistent with the ring and the two light enhancements close to the ends of the elongated structure. Since residuals are still considerable, we include an extra component into the last model (Figure 6). We choose an exponential function, since it is able to represent the likely presence of a disk in the host galaxy of a typical NLSy1 galaxy (we call it model 3). The improvement over model 2 is $\chi^2_{model3}/\chi^2_{model2} = 0.65$ for *J*-band and $\chi^2_{model3}/\chi^2_{model2} = 0.79$ for *K_s*-band. From the residual images, we observe that the ring in *J*-band (bottom panel of Figure 4) seems better defined. Moreover, in *K_s*-band (middle panel of Figure 5), hints of this structure emerge, whereas the elongated structure disappear.

The elongated feature and the light enhancements might be explained by the presence of a stellar bar showing their ansae (bright regions at the ends of bars observed in $\sim 40\%$ of SB0 galaxies, as found by Martínez-Valpuesta et al. 2007; Laurikainen et al. 2007). Such a bar could be more likely detected in *K_s*-band since neither young luminous stars or dust strongly affect its observed emission (Rix & Rieke 1993). Nevertheless, a powerful AGN, a bright bulge and a disc, might outshine the bar, making its presence less

evident. The upper panels of Figure 7 shows an image of FBQS J164442.5+261913 in *K_s*-band, with the AGN and bulge contribution subtracted (using a bulge+AGN+disc model), revealing an elongated and symmetrical feature that resembles a stellar bar over the underlying disk.

In order to confirm the existence of a bar in the host galaxy of FBQS J164442.5+261913, we perform another widely used method for detecting and describing bars; the ellipse fit of the galaxy isophotes (see plot in the lower panel of Figure 7). When ϵ and PA are plotted against radius, a bar is characterized by a local maximum in ϵ and a constant PA (typically $\Delta PA \lesssim 20^\circ$) along the bar (Wozniak et al. 1995; Jogee et al. 1999; Menéndez-Delmestre et al. 2007). We can see a region that fulfil these criteria (from $\sim 2.6'' < \text{radius} < \sim 3.2''$ and $PA \sim 78^\circ$) suggesting again the presence of a bar. Since the method of the ellipses fit also hints at the presence of a bar, we proceed to characterize its morphology (Figure 8). We add a Sérsic profile to model 3 of *K_s*-band to fit the light distribution of the stellar bar (we call it model 4). We use as initial guesses a Sérsic index $n = 0.5$ (Greene et al. 2008) and the ϵ and PA derived from the ellipse fit of Figure 7. The improvement with respect to the model where no bar is included is $\chi^2_{model4}/\chi^2_{model3} = 0.90$. From the residual image (shown in lower panel of figure 5) we can see that in general, the residuals decrease, the hints of the ring remain and the ansae are better defined. The bump remains unfitted with the functions included in the model, which is expected given that it is caused by a ring and the bar ansae. The parameters derived from every model analysed are shown in table 1.

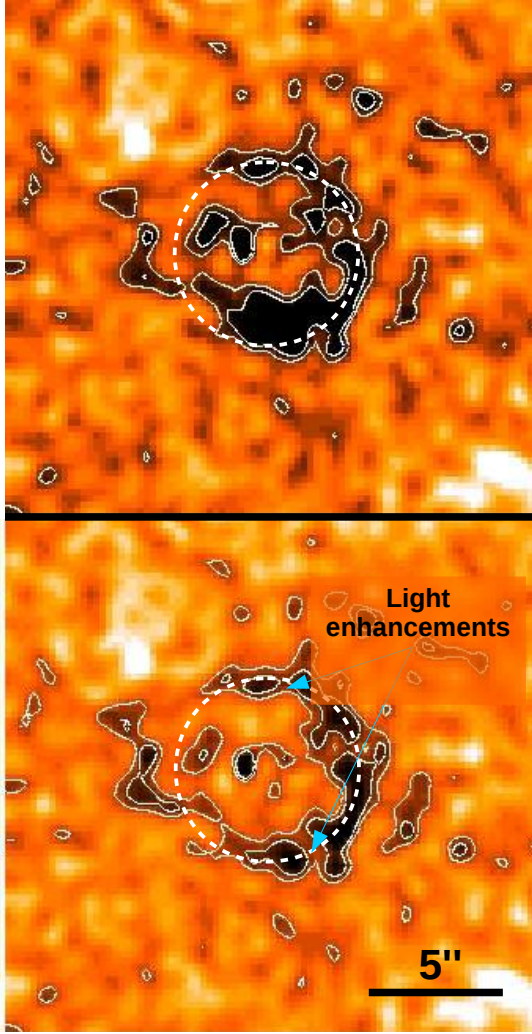


Figure 4. Residuals of the J -band model 2 (AGN+Bulge, top panel) and model 3 (AGN+Bulge+Disc, bottom panel). North is up and east is to the left. To enhance S/N and to detect faint structures, the residuals were smoothed to $< 1''$ resolution. The segmented white circle has a $3.2''$ radius and guides through the ring feature. Blue arrows show the light enhancements at the ends of the bar (ansae). A likely minor merger event feature is observed in the east part of the galaxy (from $R \approx 3''$ up to $R \approx 5''$), with a surface brightness in J -band $\mu = 21.0 \pm 0.5$ mag/arcsec², which originates the blue region at $3''$ in the $J - K_s$ colour profile of figure 9.

4.1 NIR colour gradient

Figure 9 shows the $J - K_s$ colour profile of the host galaxy of FBQS J164442.5+261913. The AGN contribution has been subtracted using the best fit model for each band. In general, as we move from the center to the outer parts of the host galaxy, we can see that the colour decreases from $J - K_s = 4.33$ mag down to $J - K_s = 3.45$ mag at $R = 1.20''$, showing that the central region (bulge) is the reddest of the host galaxy. From $R = 1.20''$ towards larger radii, the colour increases up to a local maximum of $J - K_s = 3.63$ mag at $R = 1.55''$. We link this increase in color to the bar, since here is where it has its maximum influence (see Figure 8). A second increase in colour is observed in the bar

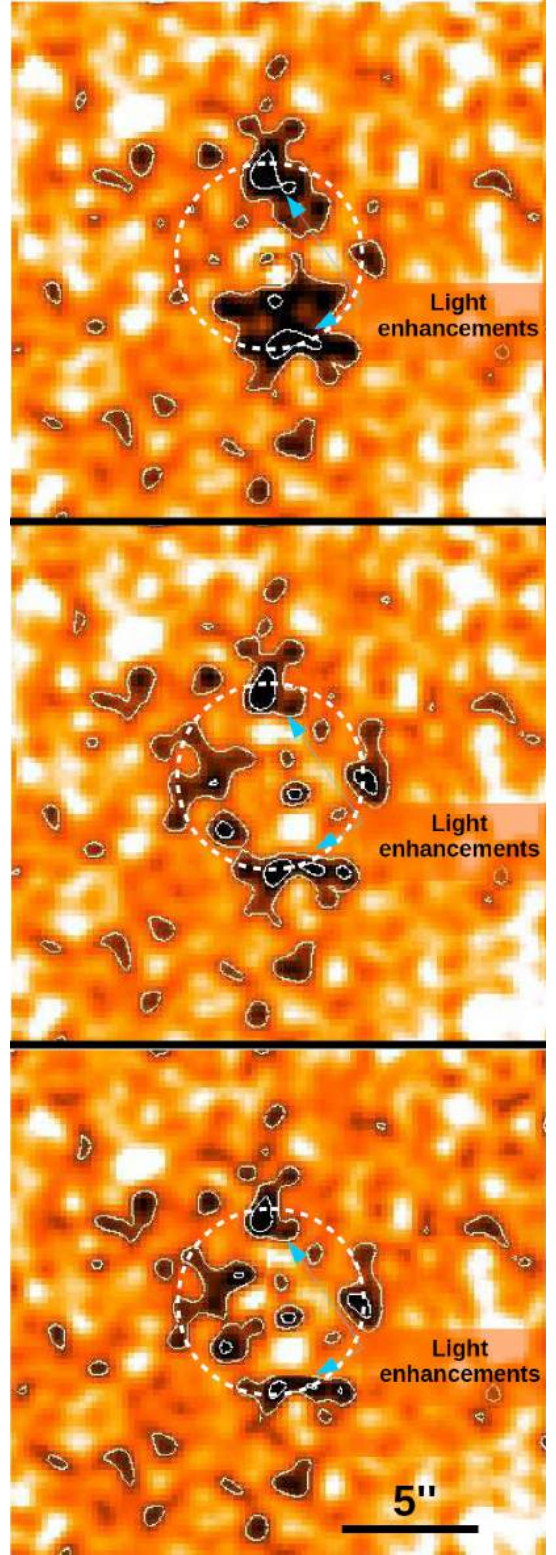


Figure 5. Residuals for the K_s -band model 2 (AGN+Bulge, top panel), model 3 (AGN+Bulge+Disc, middle panel) and model 4 (AGN+Bulge+Disc+Bar, bottom panel). North is up and east is to the left. To enhance S/N and to detect faint structures, the residuals were smoothed to $< 1''$ resolution. The segmented white circle has a $3.2''$ radius and guides through the ring feature. Blue arrows show the light enhancements at the ends of the bar (ansae). The residuals of model 2 shows hints of the bar, whereas the residuals of the models where we include a disc and a bar (model 3 and 4), show hints of the ring and the likely minor merger (eastern part of the galaxy, inside the white circle,) shown in J -band.

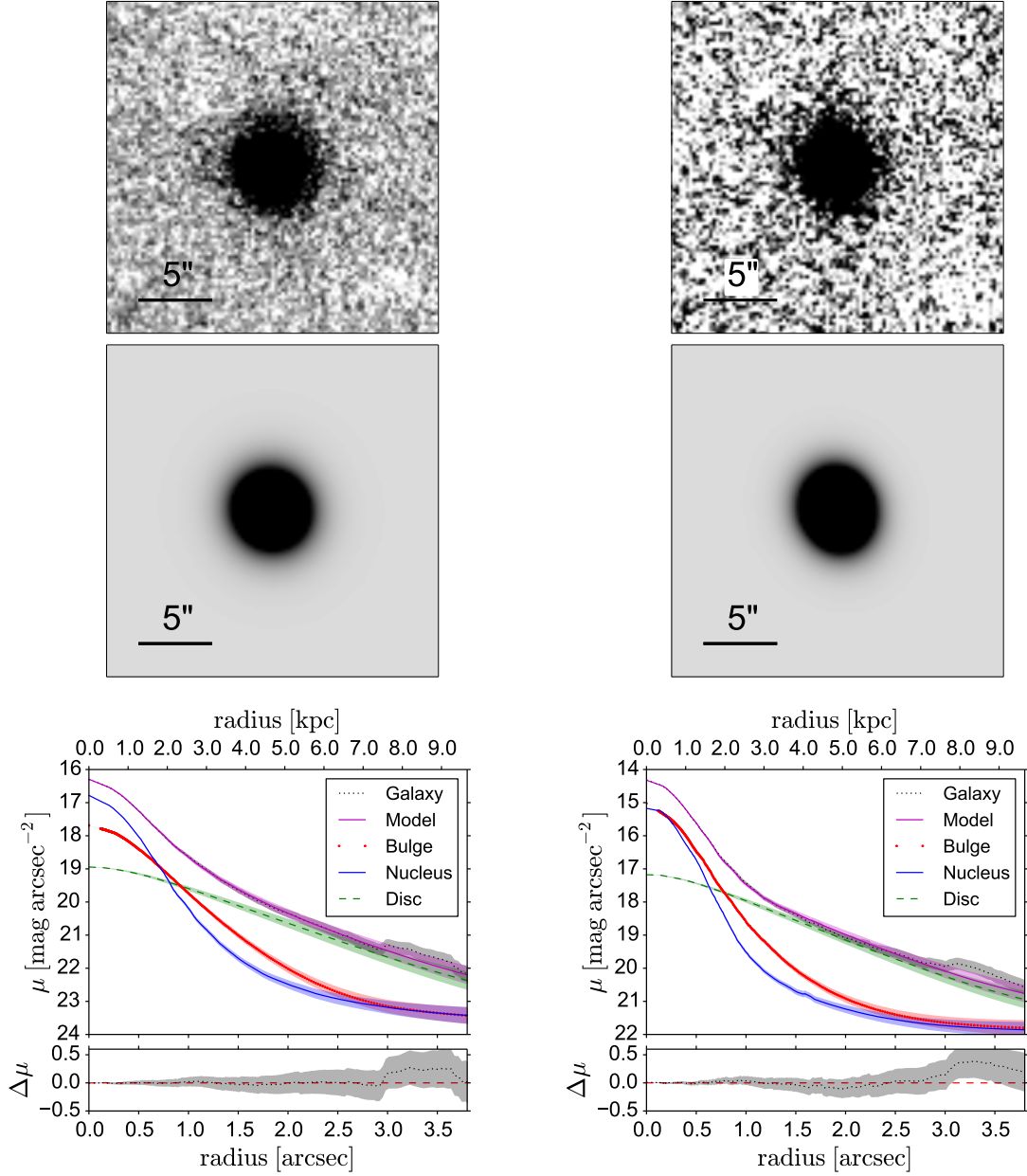


Figure 6. Model 3 (AGN+Bulge+Disc) for FBQS J164442.5+261913. Left column shows the J -band and right column shows the K_s -band. Top row shows the observed images. Middle row shows the images of our models. Lower row shows the azimuthally averaged surface brightness profiles of the target, the model and the subcomponents of the model (top panel) and its residuals (bottom panel). Symbols are explained in the plots.

region from $R = 2.20''$ to $R = 2.85''$, with a maximum of $J - K_s = 3.80$ mag. Between $2.85'' < R < 3.15''$, a blue region is observed which corresponds to eastern feature (inside the ring) in figures 4 and 5. We observe a last local minimum at $R = 3.30''$ with a colour $J - K_s = 3.80$ mag. We associate this colour to the ring, with no influence of the ansae since, according to observations by (Martínez-Valpuesta et al. 2007), ansae do not show any colour enhancement (probably because they are a dynamical phenomena). Finally, as we move outward, the disk becomes bluer, reaching an average colour $J - K_s = 3.70$ mag.

5 THE HOST GALAXY OF FBQS J164442.5+261913

According to the results shown in table 1, the host of FBQS J164442.5+261913 can be classified as a barred lenticular galaxy (SB0). In addition to the ansae morphology, that is frequent in S0 galaxies ($\sim 40\%$ of S0) as found by Laurikainen et al. (2007), both the bulge and the disc fulfil the characteristics for lenticular galaxies presented in Laurikainen et al. (2010). They also find that, as in spirals (Hunt et al. 2004; Noordermeer & van der Hulst 2007), the luminosity of the bulge in S0s correlate to

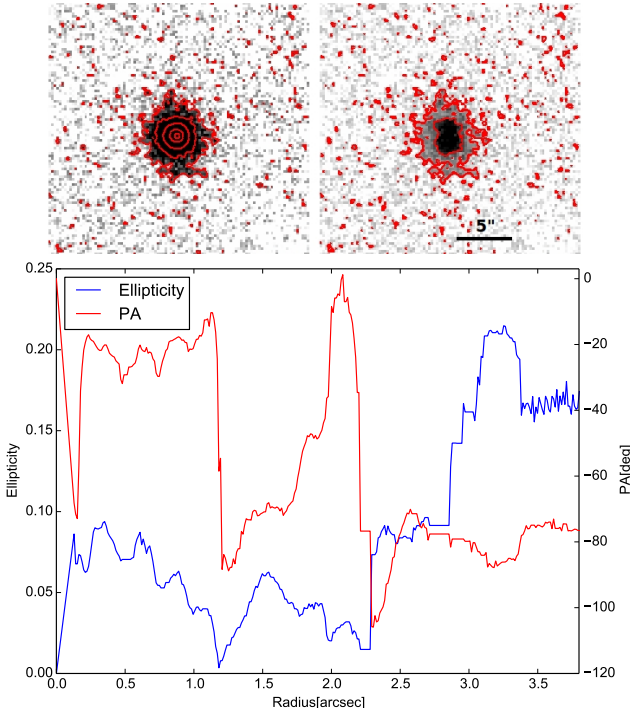


Figure 7. In top panels we compare the observed K_s -band image (top left), with an image in K_s -band where the AGN and bulge models have been subtracted (top right). The bar becomes visible on the underlying disk if the AGN and bulge contributions are subtracted. In the lower panel we show the average profiles of ellipticity ϵ (blue line) and position angle PA (red line) obtained with *ELLIPSE* from K_s -band plotted against the isophote major axis.

the luminosity of their discs. According to such correlation ($M_{K,disk} = 0.63M_{K,bulge} + 9.3$), the bulge of FBQS J164442.5+261913 should have a disk with an absolute magnitude $M_{K,disk} = -24.55 \pm 0.20$, consistent with the absolute magnitude derived through the morphological analysis in this work ($M_{K,disk} = -24.85 \pm 0.25$).

The parameters derived in this work for the components of FBQS J164442.5+261913 are consistent with those of pseudobulges. Weinzirl et al. (2009) find a connection with pseudobulges and small Sérsic indices ($n < 2.0$), consistent with $n = 1.8 \pm 0.31$ for J -band and $n = 1.9 \pm 0.35$ for K_s -band, derived for FBQS J164442.5+261913. Independently, Fisher & Drory (2008) find that pseudobulges and their discs are associated through their effective radius and scale lengths as $r_{eff}/h_r = 0.21 \pm 0.10$ consistent with FBQS J164442.5+261913 ($r_{eff}/h_r = 0.14 \pm 0.07$ for J -band and $r_{eff}/h_r = 0.14 \pm 0.06$ for K_s -band). On the contrary, they found that classical bulges have large r_{eff}/h_r ratios ($r_{eff}/h_r = 0.45 \pm 0.28$). Additionally, when we compare the structural parameters of table 1, with the results in La Barbera et al. (2010), we find that FBQS J164442.5+261913 lies below the Kormendy relation (either for J - as for K_s -band), consistent with Gadotti (2009) who find that pseudobulges do not tend to follow the Kormendy relation. Finally, if a galaxy hosts a pseudobulge, its center should be mostly population I material (young stars, gas and dust, Kormendy & Ho 2013). If we bear in mind that, in cases of high recent starburst, supergiants contribute to K -band

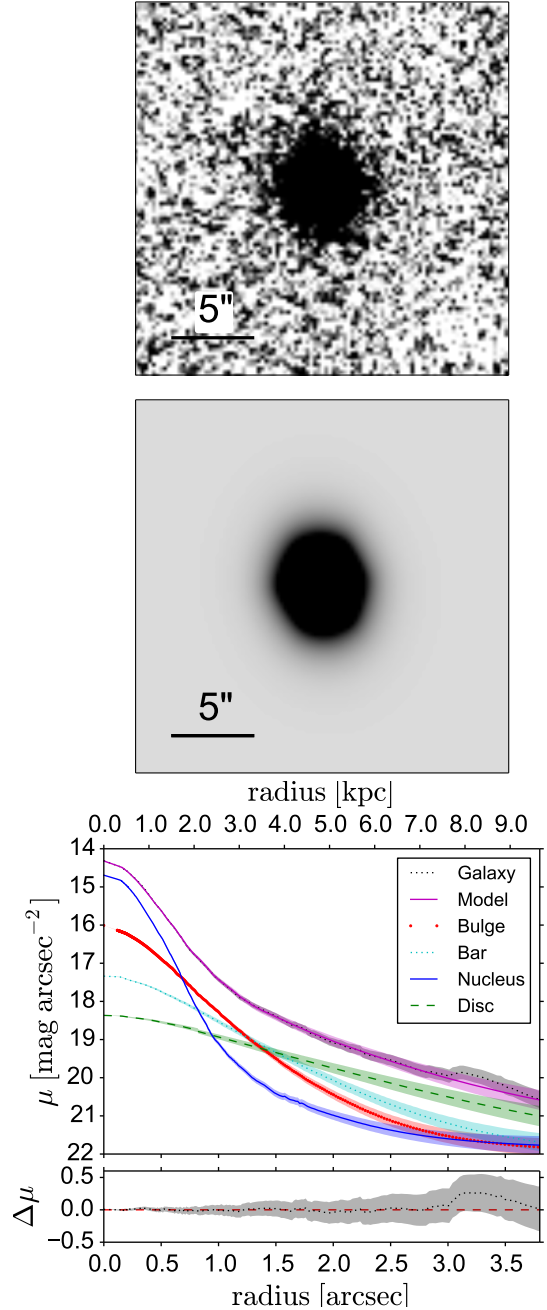


Figure 8. Model 4 (AGN+Bulge+Disc+Bar) for the K_s -band. Top panel shows the observed image. Middle panel shows our model image. Lower row shows the azimuthally averaged surface brightness profiles of the target, the model and the subcomponents of the model (top panel) and its residuals (bottom panel). Symbols are explained in the plots.

luminosity (Minniti & Rix 1996), then the $J-K_s$ color gradient of the host galaxy of FBQS J164442.5+261913, is in agreement with the latter pseudobulge classification criteria, where we see that, in the central region, K_s -band luminosity is stronger in comparison to J -band than in any other region of the galaxy.

So far, only one galaxy able to launch a relativistic jet powerful enough to accelerate particles up to γ -ray energies, is known to host a pseudobulge; PKS 2004-447 (Kotilainen

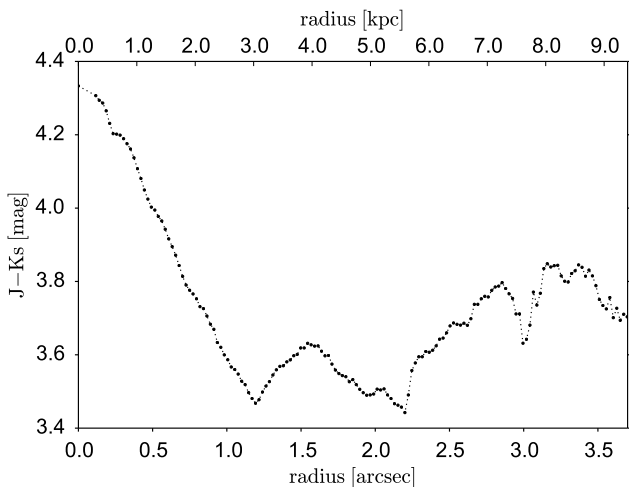


Figure 9. The radial $J - K_s$ colour profile of the host galaxy of FBQS J164442.5+261913. The AGN contribution has been subtracted from the best fit model of each band.

et al. 2016). Nevertheless, León Tavares et al. (2014) do not discard that the γ -NLSy1 1H 0323+342 is also hosted by a pseudobulge.

We now evaluate whether the parameters derived for the bar in FBQS J164442.5+261913 are in accordance with those for active early-type galaxies. Using the maximum ellipticity of the ellipse fits to the bar region as bar length (Marinova & Jogee 2007), we find that the length of the bar in FBQS J164442.5+261913 is $r_{bar} = 8.13 \text{ kpc} \pm 0.25$, if we normalized it to the disc scale length h_r , we obtain $r_{bar}/h_r = 1.00 \pm 0.06$. On the other hand, we can calculate the bar strength f_{bar} (Abraham & Merrifield 2000, see also Whyte et al. 2002; Aguerri et al. 2009; Laurikainen et al. 2007; Hoyle et al. 2011) defined as:

$$f_{bar} = \frac{2}{\pi} \left\{ \arctan \left[(b/a)^{-0.5} \right] - \arctan \left[(b/a)^{0.5} \right] \right\} \quad (3)$$

where b/a is the minor to major axis ratio of the bar. We obtain a bar strength $f_{bar} = 0.17 \pm 0.03$. According to e.g. Aguerri et al. (2009) and Laurikainen et al. (2007), the bar in FBQS J164442.5+261913 is long and weak, consistent with S0 galaxies as found by (Laurikainen et al. 2002).

The bar in FBQS J164442.5+261913 might be related to the ring through resonances (Athanasoula et al. 2010, and references therein), given that secular evolution is likely the main evolutionary process that is currently in progress in its host galaxy. Therefore, the ring-like feature might be the result of gas redistribution by angular momentum transport driven by the bar (i.e. a ring constructed by a rotating bar interacting with the disk gas). In this scenario, the gas is moved by the bar into orbits near dynamical resonances (for a review, see Athanasoula et al. 2013).

The main resonances are the Inner Lindblad Resonance (ILR) $\Omega_{ILR} = \Omega_{bar} - \kappa/2$, the Outer Lindblad Resonance (OLR) $\Omega_{OLR} = \Omega_{bar} + \kappa/2$ (Buta & Combes 1996) and the Ultra Harmonic Resonance (UHR) $\Omega_{UHR} = \Omega_{bar} - \kappa/4$, where Ω_{bar} is the bar pattern speed and κ is the epicyclic

frequency (Lindblad 1974). The latter is located close to corotation (Sellwood 2013), i.e. where the disc and the bar corotate.

Observations state that bars end near corotation (Kent 1987; Sempere et al. 1995; Merrifield & Kuijken 1995; Gerssen et al. 1999; Debattista & Williams 2001; Gerssen 2002; Corsini et al. 2003), and can drive structures such as inner rings approximately at the UHR (Kormendy & Kennicutt 2004). Therefore, the feature located at $R = 3.20''$, might be consistent with that of an inner ring.

Another scenario for the ring formation in FBQS J164442.5+261913 is a minor merger event. Athanasoula et al. (1997) show that the interaction of a small satellite galaxy on a barred galaxy can produce a ring that encloses the bar. Also, (Mapelli et al. 2015) show that minor mergers with gas-rich satellites might explain the formation of rings in lenticular galaxies. This scenario is supported by the residuals in J -band (see Figure 4), where a feature of surface brightness $\mu = 21.0 \pm 0.5 \text{ mag/arcsec}^2$ is shown about $\sim 5.15''/13.10 \text{ kpc}$ east from the center of FBQS J164442.5+261913 (resembling the Seyfert galaxy NGC 1097 whose light distribution is strongly affected by a small satellite galaxy, Higdon & Wallin 2003). This feature seems to interrupt the shape of the ring in the eastern part of the galaxy and even cause the color enhancement at $3.0''$.

An alternative and more likely scenario was proposed by Marino et al. (2011) for their sample of lenticular galaxies. The formation of the ring might be a joint effect of secular evolution driven by the bar and gas accreted from a small satellite galaxy (or many). Moreover, since S0 galaxies lack of an own gas reservoir (unlike spirals), this scenario also explains the origin of the gas needed to grow a massive bulge ($M_J = -22.42 \pm 0.40$ and $M_{K_s} = -24.21 \pm 0.32$) and activate the black hole in FBQS J164442.5+261913, as well as the way this gas is channelled to the most central parts of the galaxy (i.e. through angular momentum transport driven by the bar, Shlosman et al. 1990; Ohta et al. 2007).

We finally observe that the parameters of the bar and the ring hosted by FBQS J164442.5+261913, are similar to the bar of PKS 2004-447 (Kotilainen et al. 2016) and the ring in 1H 0323+342 (León Tavares et al. 2014). While the bars of PKS 2004-447 and FBQS J164442.5+261913, are $r_{bar} \approx 7.80 \text{ kpc}$ and $r_{bar} = 8.13 \pm 0.25 \text{ kpc}$ (taking the length of the bar as the maximum in the ellipticity profile), respectively, with absolute K_s -band magnitude of $K_{bar} = -23.44 \pm 0.38$ and $K_{bar} = -23.86 \pm 0.52$, respectively; the rings of 1H 0323+342 and FBQS J164442.5+261913, are $\sim 8.24 \text{ kpc}$ and $\sim 8.13 \text{ kpc}$, respectively. Moreover, PKS 2004-447 shows an arm-like feature, whose origin might be related to a minor merger event (see Figure 19 of Athanasoula et al. 1997) and that, at some point, might become a ring, similar to the feature shown in FBQS J164442.5+261913.

According to the most accepted processes for jet formation, the Blandford–Znajek (BZ, Blandford & Znajek 1977; MacDonald & Thorne 1982; Penna et al. 2013) and the Blandford–Payne (BP, Blandford & Payne 1982) mechanisms, the jet launching and collimation requires very massive black holes with high spins and strong magnetic fields. All of this require major mergers to occur, which fits well with previous observations (McLure et al. 2004; Sikora et al. 2007) and the jet formation paradigm (where powerful rel-

ativistic jets are launched from giant elliptical galaxies, Marscher 2009). However, it comes completely at odds with the morphology of FBQS J164442.5+261913, with a bar and a disc, that lacks of a classical bulge and with a black hole mass (as estimated by the FWHM of its BLR lines and the continuum luminosity, Yuan et al. 2008) $M_{BH} \sim 8 \times 10^6 M_{\odot}$ (although, previous studies show that values $M_{BH} \gtrsim 10^8 M_{\odot}$ could be obtained when estimating its black hole mass by different methods, Baldi et al. 2016; Calderone et al. 2013).

6 SUMMARY

We have performed a detailed photometric analysis of the γ -NLSy1 FBQS J164442.5+261913. We use deep near-infrared imagery in J - and K_s -bands taken with the near-infrared camera NOTcam on the NOT. The main results of this analysis are:

- The surface brightness distribution of FBQS J164442.5+261913 is best fitted by a model resulting from a sum of a nuclear source, a bulge and a disc. Additionally to these components, a stellar bar in the K_s -band image is detected and modeled. The morphological parameters derived from our analysis show that the bulge, the disk and the bar of the host galaxy of FBQS J164442.5+261913 fulfil the characteristics of SB0 galaxies.

- We find that the Sérsic index and the relations between bulge and disc for FBQS J164442.5+261913 are in good agreement with those of pseudobulges. Therefore, the bulge in the host galaxy of FBQS J164442.5+261913 is statistically most likely to be pseudo.

- In both J - and K_s -bands, we detect a ring enclosing the bar that is interrupted by, what it seems to be, a recent minor merger which might hint to the formation process of such inner ring, as suggested by Athanassoula et al. (1997).

- When comparing the ring and bar in FBQS J164442.5+261913 to the ring and bar in 1H 0323+342 and PKS 2004-447 (the only two γ -NLSy1 whose morphology have been analysed until now), we find similarities regarding size and magnitude. Likewise, PKS 2004-447 shows an arm-like feature, whose origin might be related to a minor merger event and that, at some point, might become a ring, similar to the inner ring in FBQS J164442.5+261913.

We conclude that the prominent bar in the host galaxy of FBQS J164442.5+261913 has mostly contributed to its overall morphology driving a strong secular evolution, which plays a crucial role in the onset of the nuclear activity and the growth of its massive (pseudo) bulge. Minor mergers, in conjunction, are likely to provide the necessary fresh supply of gas to the central regions of the host galaxy.

Although our findings strongly suggest that secular evolution is the main process taking place in FBQS J164442.5+261913, our available data is insufficient to address some other questions as whether its (pseudo) bulge shows an increased star formation activity or if it is rotation-dominated (as it should, given its disky origin; Kormendy & Ho 2013). Therefore, we encourage different wavelengths imaging and integral field spectroscopy (IFS) observations to this galaxy and the whole sample of radio-loud NLSy1s.

ACKNOWLEDGEMENTS

We thank Kari Nilsson who provided expertise that assisted this work. We acknowledge support by CONACyT research grant 151494 (Mexico), CONACyT program for PhD studies and Finnish Centre for Astronomy with ESO (FINCA). This research is based on observations made with the Nordic Optical Telescope, operated by the Nordic Optical Telescope Scientific Association at the Observatorio del Roque de los Muchachos, La Palma, Spain, of the Instituto de Astrofísica de Canarias. This publication makes use of data products from the Two Micron All Sky Survey.

REFERENCES

- Abdo A. A., et al., 2009, *ApJ*, **707**, L142
 Abraham R. G., Merrifield M. R., 2000, *AJ*, **120**, 2835
 Aguerri J. A. L., Méndez-Abreu J., Corsini E. M., 2009, *A&A*, **495**, 491
 Antón S., Browne I. W. A., Marchã M. J., 2008, *A&A*, **490**, 583
 Athanassoula E., Puerari I., Bosma A., 1997, *MNRAS*, **286**, 284
 Athanassoula E., Romero-Gómez M., Bosma A., Masdemont J. J., 2010, *MNRAS*, **407**, 1433
 Athanassoula E., Machado R. E. G., Rodionov S. A., 2013, *MNRAS*, **429**, 1949
 Bade N., Fink H. H., Engels D., Voges W., Hagen H.-J., Wisotzki L., Reimers D., 1995, *A&AS*, **110**, 469
 Baldi R. D., Capetti A., Robinson A., Laor A., Behar E., 2016, *MNRAS*, **458**, L69
 Barazza F. D., Jogee S., Marinova I., 2008, *ApJ*, **675**, 1194
 Bertin E., Arnouts S., 1996, *A&ASS*, **117**, 393
 Blandford R. D., Payne D. G., 1982, *MNRAS*, **199**, 883
 Blandford R. D., Znajek R. L., 1977, *MNRAS*, **179**, 433
 Bruce V. A., et al., 2012, *MNRAS*, **427**, 1666
 Buta R., Combes F., 1996, *Fundamentals Cosmic Phys.*, **17**, 95
 Calderone G., Ghisellini G., Colpi M., Dotti M., 2013, *MNRAS*, **431**, 210
 Corsini E. M., Debattista V. P., Aguerri J. A. L., 2003, *ApJ*, **599**, L29
 Crenshaw D. M., Kraemer S. B., Gabel J. R., 2003a, *AJ*, **126**, 1690
 Crenshaw D. M., Kraemer S. B., Gabel J. R., 2003b, *AJ*, **126**, 1690
 Debattista V. P., Williams T. B., 2001, in Funes J. G., Corsini E. M., eds, *Astronomical Society of the Pacific Conference Series Vol. 230, Galaxy Disks and Disk Galaxies*. pp 553–554 ([arXiv:astro-ph/0009302](https://arxiv.org/abs/astro-ph/0009302))
 Elmegreen B. G., Elmegreen D. M., Hirst A. C., 2004, *ApJ*, **612**, 191
 Fisher D. B., Drory N., 2008, in Funes J. G., Corsini E. M., eds, *Astronomical Society of the Pacific Conference Series Vol. 396, Formation and Evolution of Galaxy Disks*. p. 309
 Gadotti D. A., 2009, *mnras*, **393**, 1531
 Gerssen J., 2002, in Athanassoula E., Bosma A., Mujica R., eds, *Astronomical Society of the Pacific Conference Series Vol. 275, Disks of Galaxies: Kinematics, Dynamics and Perturbations*. pp 197–200
 Gerssen J., Kuijken K., Merrifield M. R., 1999, *MNRAS*, **306**, 926
 Graham A. W., Driver S. P., 2005, *PASP*, **22**, 118
 Greene J. E., Ho L. C., Barth A. J., 2008, *ApJ*, **688**, 159
 Häussler B., et al., 2007, *ApJS*, **172**, 615
 Higdon J. L., Wallin J. F., 2003, *ApJ*, **585**, 281
 Hoyle B., et al., 2011, *MNRAS*, **415**, 3627
 Hunt L. K., Pierini D., Giovanardi C., 2004, *A&A*, **414**, 905
 Jogee S., Kenney J. D. P., Smith B. J., 1999, *ApJ*, **526**, 665

- Kaspi S., Smith P. S., Netzer H., Maoz D., Jannuzi B. T., Giveon U., 2000, *ApJ*, **533**, 631
- Kent S. M., 1987, *AJ*, **93**, 1062
- Knapen J. H., Shlosman I., Peletier R. F., 2000, *ApJ*, **529**, 93
- Kormendy J., Ho L. C., 2013, *ARA&A*, **51**, 511
- Kormendy J., Kennicutt Jr. R. C., 2004, *ARA&A*, **42**, 603
- Kotilainen J. K., Hyvönen T., Falomo R., Treves A., Uslenghi M., 2011, *A&A*, **534**, L2
- Kotilainen J. K., León-Tavares J., Olguín-Iglesias A., Baes M., Anorve C., Chavushyan V., Carrasco L., 2016, *ApJ*, **832**, 157
- La Barbera F., de Carvalho R. R., de La Rosa I. G., Lopes P. A. A., 2010, *MNRAS*, **408**, 1335
- Laine S., Shlosman I., Knapen J. H., Peletier R. F., 2002, *ApJ*, **567**, 97
- Laor A., 2000, *ApJ*, **543**, L111
- Laurikainen E., Salo H., Rautiainen P., 2002, *MNRAS*, **331**, 880
- Laurikainen E., Salo H., Buta R., Knapen J. H., 2007, *MNRAS*, **381**, 401
- Laurikainen E., Salo H., Buta R., Knapen J. H., Comerón S., 2010, *MNRAS*, **405**, 1089
- León Tavares J., et al., 2014, *ApJ*, **795**, 58
- Lindblad P. O., 1974, in Shakeshaft J. R., ed., IAU Symposium Vol. 58, The Formation and Dynamics of Galaxies. pp 399–411
- MacDonald D., Thorne K. S., 1982, *MNRAS*, **198**, 345
- Mapelli M., Rampazzo R., Marino A., 2015, *A&A*, **575**, A16
- Marino A., Bianchi L., Rampazzo R., Thilker D., Annibali F., Bressan A., Buson L. M., 2011, *Ap&SS*, **335**, 243
- Marinova I., Jogee S., 2007, *ApJ*, **659**, 1176
- Marscher A. P., 2009, in Lecture Notes in Physics 794, ed. T. Belloni, 173
- Martínez-Valpuesta I., Knapen J. H., Buta R., 2007, *AJ*, **134**, 1863
- Mathur S., Fields D., Peterson B. M., Grupe D., 2012a, *ApJ*, **754**, 146
- Mathur S., Fields D., Peterson B. M., Grupe D., 2012b, *ApJ*, **754**, 146
- Mattox J. R., et al., 1996, *ApJ*, **461**, 396
- McLure R. J., Willott C. J., Jarvis M. J., Rawlings S., Hill G. J., Mitchell E., Dunlop J. S., Wold M., 2004, *MNRAS*, **351**, 347
- Menéndez-Delmestre K., Sheth K., Schinnerer E., Jarrett T. H., Scoville N. Z., 2007, *ApJ*, **657**, 790
- Merrifield M. R., Kuijken K., 1995, *MNRAS*, **274**, 933
- Minniti D., Rix H. W., 1996, in Spiral Galaxies in the Near-IR. Proceedings of the ESO/MPA Workshop Held at Garching, Germany, 7–9 June 1995
- Noordermeer E., van der Hulst J. M., 2007, *MNRAS*, **376**, 1480
- Ohta K., Aoki K., Kawaguchi T., Kiuchi G., 2007, *ApJS*, **169**, 1
- Olguín-Iglesias A., et al., 2016, *MNRAS*, **460**, 3202
- Orban de Xivry G., Davies R., Schartmann M., Komossa S., Marconi A., Hicks E., Engel H., Tacconi L., 2011, *MNRAS*, **417**, 2721
- Osterbrock D. E., Pogge R. W., 1985, *ApJ*, **297**, 166
- Peng C. Y., Ho L. C., Impey C. D., Rix H.-W., 2011, GALFIT: Detailed Structural Decomposition of Galaxy Images, Astrophysics Source Code Library (ascl:1104.010)
- Penna R. F., Narayan R., Sądowski A., 2013, *MNRAS*, **436**, 3741
- Pogge R. W., 2000, *New Astron. Rev.*, **44**, 381
- Rix H.-W., Rieke M. J., 1993, *ApJ*, **418**, 123
- Sellwood J. A., 2013, Dynamics of Disks and Warps. p. 923, doi:10.1007/978-94-007-5612-0_18
- Sempere M. J., Combes F., Casoli F., 1995, *A&A*, **299**, 371
- Sheth K., Regan M. W., Scoville N. Z., Strubbe L. E., 2003, *ApJ*, **592**, L13
- Shlosman I., Begelman M. C., Frank J., 1990, *Nature*, **345**, 679
- Sikora M., Stawarz L., Lasota J.-P., 2007, *ApJ*, **658**, 815
- Skrutskie M. F., et al., 2006, *AJ*, **131**, 1163
- Weinzirl T., Jogee S., Khochfar S., Burkert A., Kormendy J., 2009, *ApJ*, **696**, 411
- Whyte L. F., Abraham R. G., Merrifield M. R., Eskridge P. B., Frogel J. A., Pogge R. W., 2002, *MNRAS*, **336**, 1281
- Wozniak H., Friedli D., Martinet L., Martin P., Bratschi P., 1995, *A&AS*, **111**, 115
- Yuan W., Zhou H. Y., Komossa S., Dong X. B., Wang T. G., Lu H. L., Bai J. M., 2008, *ApJ*, **685**, 801

This paper has been typeset from a $\text{\TeX}/\text{\LaTeX}$ file prepared by the author.